THE ASTROPHYSICAL JOURNAL, 437:L95–L98, 1994 December 20


# A SEARCH FOR DIFFUSE Hα EMISSION FROM Lyα ABSORPTION CLOUDS TOWARD 3C 273

J. BLAND-HAWTHORN AND K. TAYLOR
Anglo-Australian Observatory, P.O. Box 296, Epping, NSW 2121, Australia
S. VEILLEUX
Kitt Peak National Observatory, Tucson, AZ 85726-6732
AND
P. L. SHOPBELL
Department of Space Physics & Astronomy, Rice University, Houston, TX 77251-1892
*Received 1994 July 1; accepted 1994 October 3*

## ABSTRACT

The *Hubble Space Telescope* has identified a series of low-velocity Lyα absorption lines in the direction of 3C 273. We have investigated a recent claim (Williams & Schommer 1993) that there is diffuse Hα emission with surface brightness $1.2 \times 10^{-18}$ ergs cm$^{-2}$ s$^{-1}$ arcsec$^{-2}$ at a radial velocity within 130 km s$^{-1}$ of one of these Lyα features. The observations were made with the TAURUS-2 imaging Fabry-Perot interferometer and a Tek 1024$^2$ CCD at the 3.9 m Anglo-Australian Telescope. We do not detect Hα emission at the claimed wavelength λ6600.3 down to a 3 σ upper limit of $4 \times 10^{-19}$ ergs cm$^{-2}$ s$^{-1}$ arcsec$^{-2}$ ($E_m \approx 0.2$ cm$^{-6}$ pc), nor do we detect emission at the absorption-line velocity. We show that the Jacquinot advantage of spectroscopic interferometers makes 3 σ detection thresholds as low as $E_m$(Hα) = 0.02 cm$^{-6}$ pc quite feasible. Even at this very deep limit, it is unlikely that Lyα absorbers irradiated by the UVX background will be detectable in optical line emission at any redshift. However, our sensitivity limit now brings other important detections into the realm of possibility for the first time, in particular, the detection of ionized disks beyond the H I truncation radius in spiral galaxies.

*Subject headings:* intergalactic medium — quasars: absorption lines — quasars: individual (3C 273) — techniques: interferometric — techniques: spectroscopic

## 1. INTRODUCTION

Quasar absorption lines have traditionally been used to probe the formation and evolution of low mass structures at cosmological redshifts (Lanzetta 1993). However, the *Hubble Space Telescope* (*HST*) has now revealed substantial numbers of Lyα absorption line systems at low redshift toward 3C 273 (Bahcall et al. 1991; Morris et al. 1991). Since the intervening clouds have not been seen at H I λ21 cm, it is often assumed that detecting optical emission from these clouds is beyond the scope of modern-day spectrographs (Weymann 1993).

In recent months, Williams & Schommer (1993) have claimed to detect diffuse Hα emission within a few angstroms of the 1580 km s$^{-1}$ Lyα feature (Bahcall et al. 1991). The potential importance of this result is hard to overstate since, if confirmed, it now becomes possible to examine a wide range of spectroscopic diagnostics to determine, inter alia, cloud pressures, density profiles, and morphologies. In addition, the Lyα absorbers can be used to probe the ultraviolet background as a function of redshift (Hogan & Weymann 1987). Thus, we have attempted to confirm the Williams-Schommer detection. In this *Letter*, we describe the TAURUS-2 observations, the stages of reduction, and the implications of our new results. Finally, we discuss the practical limits for Fabry-Perot interferometry in the context of detecting diffuse sources, particularly Lyα absorption clouds at high redshift.

## 2. OBSERVATIONS

TAURUS-2 (Taylor & Atherton 1980) was used with the Tek 1024$^2$ CCD (read noise, $\sigma_R = 2.3e^-$) at the f/8 Cassegrain focus of the 3.9 m Anglo-Australian Telescope. The system was fully calibrated during the nights of 1994 March 7–8 prior to two photometric, dark nights on 1994 March 9–10. A high-finesse, 50 mm diameter etalon with 57 Å free spectral range and 40 μm optical gap was borrowed from the HIFI system (Bland & Tully 1989). The TAURUS-2 optics produce a pupil size of 59.9 mm coincident with the etalon cavity. A 45.0 mm pupil stop is placed close to the 55.0 mm clear etalon aperture to ensure that the pupil falls within the coated area for all field angles. All surfaces in the optical train, including the Tek chip, are antireflection-coated to better than 1.5%.

We went to great lengths to ensure that the system was free of the various ghost families that have plagued other Fabry-Perot observations in the past. A plate drilled with 100 μm holes spaced 10.0 mm apart was placed in focus at the focal plane. When illuminated with a white-light source, the grid pattern indicates how the etalon must be tilted to remove the ghost reflections down to third or fourth order within the field of interest. The "extraneous etalon" effect, due to the resonating plate cavities, produced a fringe pattern with a considerably smaller amplitude than the CCD fringes. The narrow-band filters were placed out of focus close to the focal plane.

We exposed for 1.5 hr on a 5.′5 × 5.′5 field centered on 3C 273 in five separate exposures at the same etalon spacing. The same exposure times were used to observe two blank sky fields at the same airmass in five exposures. Full monochromatic (Ne) and white-light (W) observations were taken for the photometric (Bland-Hawthorn 1994) and wavelength calibration procedures (Bland & Tully 1989). In addition, we observed a flux standard (η Hya) and a planetary nebula (IC 2165) in order to check the photometric calibration. The "effective photometric bandpass" of the HIFI etalon was measured to be 1.80 ± 0.07 Å from the monochromatic calibration cube, while the overall system efficiency was found to be 13.5% ± 0.5% (instrument + CCD + telescope). A four-period (top-hat) filter with central wavelength λ6594 and bandwidth 55 Å was used for all observations. The 50 × 50 mm

filters limited the field of view to 334″ at a scale of 0.594″ pixel$^{-1}$.

## 3. ANALYSIS

After bias subtraction, each of the frames was treated with a flat-field image to divide out the pronounced CCD fringes. The flat-field image was obtained by white-light illumination of the dome in a series of exposures at the same etalon spacing. The fringe pattern was seen to change even when tuning the etalon by a few angstroms. After 3 × 3 median smoothing, the noise level of the flat field was less than 0.25%. No attempt was made to remove pixel-pixel variations. The low-frequency variations of the flat field were removed with twilight sky observations in order to correct for uneven illumination and vignetting effects within the dome flats. Point sources and cosmic-ray events were removed by masking; these constituted about 1% of the imaged area.

After fitting the incomplete airglow rings to find the optical axis, the data were transformed from a Cartesian to a polar coordinate frame before summing along one axis to produce the final spectrum. The polar coordinate frame showed weak evidence for moiré fringes, but these are unlikely to affect significantly the noise structure of the final spectra. The optical axis was determined for each image to about 0.2 pixel which is a wavelength error smaller than 0.1 Å over the full field.

The azimuthally summed data produce spectra with quadratic sampling. These were transformed to linear sampling by fitting to the three bright OH lines and performing spline interpolation. The interpolation preserved the original number of spectral channels (~600) and conserved the flux within equal spectral intervals. The autocorrelation of the sky spectra with the on-object spectra demonstrated that the rms wavelength calibration was good to about 0.3 pixel. The wavelength dispersion ($\delta\lambda$) of the final spectra was measured to be 0.0676 Å pixel$^{-1}$. Finally, all spectra were calibrated in units of exo-atmospheric flux using the conversion factor determined from the photometric standards.

## 4. RESULTS

In Figure 1, we present the on-object and off-object (blank sky) spectra. The angular dispersion, $d\lambda/d\theta = -\lambda \tan\theta$, causes the rings near the optical axis to be heavily oversampled and the rings at the edge of the field to be close to optimum sampling. The spectral sensitivity redward of λ6582 is constant; at shorter wavelengths, the rings are seriously incomplete. The vertical bars indicate the expected positions for Hα associated with (*a*) the 1010 km s$^{-1}$ and (*b*) the 1580 km s$^{-1}$ Lyα features. In Figure 2, we magnify the wavelength region discussed by Williams & Schommer (1993) and show the difference of the on-object and off-object spectra. The off-object spectrum combines data from both nights. To get a good match between the OH lines, we needed to scale up the off-object (sky) spectrum by a constant factor of 1.58.

Williams & Schommer (1993) identified a feature with a flux of 1.2 × 10$^{-18}$ ergs cm$^{-2}$ s$^{-1}$ arcsec$^{-2}$ [$E_m$(Hα) ≈ 0.58 cm$^{-6}$ pc] at a wavelength of λ6600.3. In Figure 2, note that the continuum is particularly clean between the two red OH lines in both spectra and that no such feature is evident. Rather than subtracting an off-object spectrum, Williams & Schommer fitted an Airy function to both OH lines which they subtract from the observed spectrum. This produces a somewhat higher signal-to-noise ratio in their residual spectrum. In a 90 minute combined exposure, we are able to detect an Hα emission measure of 0.2 cm$^{-6}$ pc at the 3 σ level with respect to the flat

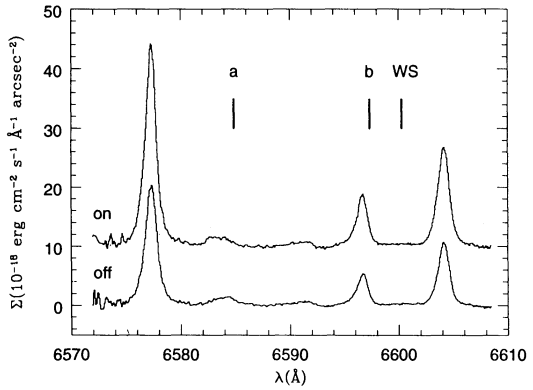


FIG. 1.—A comparison of the on-object (3C 273) and off-object spectra; a constant offset of 3.2 × 10$^{-18}$ ergs cm$^{-2}$ s$^{-1}$ Å$^{-1}$ arcsec$^{-2}$ has been subtracted from the off-object spectrum. The three highly variable OH airglow lines λλ6577.28, 6596.64, 6604.13 (Osterbrock & Martel 1992) are seen, along with weak unidentified features at λ6591 and λ6583, in both the on-object and off-object fields. The asymmetric λ6591 feature is found to be stable in all frames, in contrast to the λ6583 feature which exhibits a varying profile from frame to frame. The vertical bars *a* and *b* indicate the velocities of the Lyα absorption features identified by the *HST*; the position of the Williams & Schommer "detection" is also indicated (WS).

background. The weak positive features in our residual spectrum at λ6596.5 ($R_1$) and λ6605 ($R_2$) are artefacts of the sky subtraction. $R_1$ and $R_2$ have emission measures of 0.10 and 0.35 cm$^{-6}$ pc and have a statistical significance of 0.9 σ and 3.4 σ, respectively, when expressed in terms of the residual noise after sky subtraction. We are able to rule out the Williams-Schommer detection at the level of 5.7 σ with respect to our sky-subtracted residual, and at the level of 8.0 σ with respect to a theoretical fit to our data. Unfortunately, the low-redshift absorption line identified by the *HST* falls on the atmospheric λ6583 feature. In Figure 1, it is intriguing to note that there is weak structure on the blue wing of this line. However, the λ6583 feature was found to be fairly unstable between the different exposures with line structure varying on short time-

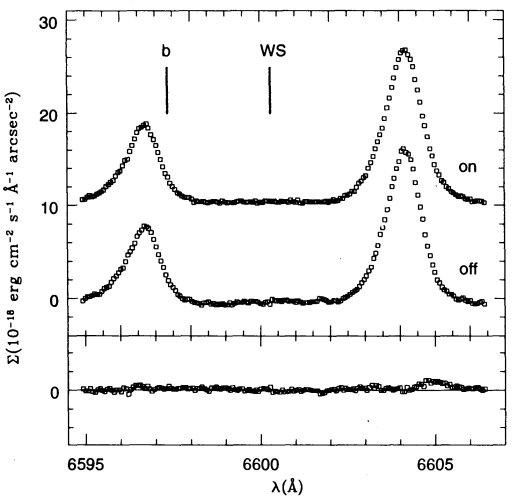


FIG. 2.—An expanded view of the spectral region (see Fig. 1) between the red OH lines in the on-object and off-object spectra. The sky-subtracted residual spectrum is shown in the lower panel. The residual features at λ6596.5 and λ6605 are artefacts of the sky subtraction. The Williams & Schommer "detection" is roughly twice the strength of the red artefact. Our sky-subtracted residual shows that no such feature occurs at their detection wavelength of λ6600.3. A constant offset of 6.8 × 10$^{-18}$ ergs cm$^{-2}$ s$^{-1}$ Å$^{-1}$ arcsec$^{-2}$ has been subtracted from the residual spectrum.

scales. A formal 3 $\sigma$ upper limit at the low-redshift absorption line velocity is $E_m(\mathrm{H}\alpha) \approx 2.0\,\mathrm{cm}^{-6}$ pc.

Our technique is very much more sensitive to this experiment for a number of reasons. First, the angular dispersion of the Rutgers system allows through only 6 Å at each etalon spacing. To obtain an adequate spectral baseline, the field had to be observed at a number of different etalon spacings. The spectra were then joined to obtain the final spectrum which, as the authors acknowledge, is particularly hazardous in light of the rapidly varying nature of atmospheric OH transitions. The TAURUS-2 optics, when using 50 mm etalon and filters, allow 40 Å to be dispersed across the detector so that the required spectral coverage is obtained in a single exposure. Second, the effective finesse of our etalon was $52 \pm 2$ which is a factor of 1.7 higher than the finesse of the Rutgers etalon used for the 3C 273 experiment. Since a higher finesse increases the contrast between the peak and the trough quadratically, this has the important consequence of suppressing the wings of the instrumental Airy function by a factor of 3. Furthermore, our spectral resolution ($\Gamma = 1.1 \pm 0.04$ Å FWHM) permits a much better separation of the OH lines than was possible with the Rutgers setup (2.4 Å FWHM). What is not evident from Figure 1 in Williams & Schommer (1993) is that the region between the two bright OH lines does not reach the continuum baseline due to their low spectral resolution and the large wings in their instrumental profile. This is clearly not the case in our observations (Fig. 2). More importantly, and the likely reason for the positive detection at two telescopes, the configuration used by these authors will transmit a variety of first-order ghost reflections which cannot be adequately corrected for. Observations of the active galaxy NGC 1068 taken with the Rutgers Fabry-Perot in 1989 March confirm that all of the dominant ghost families arise within this system. We have run a wide range of simulations using the observational parameters specific to the Rutgers system to show how such anomalies can produce a spurious positive detection.

## 5. DETECTION LIMITS

We now address the issue of whether the Jacquinot advantage of Fabry-Perots is sufficient to probe the cosmic radiation bath. Specifically, what is the practical flux limit of the Fabry-Perot technique, and is this deep enough to be useful? In the small angle approximation, the equation of constructive interference, $m\lambda = 2\mu l \cos\theta$, leads to the important result

$$\theta^2 = \frac{2}{\mathscr{R}} = \frac{\Omega}{\pi}, \tag{1}$$

where $\mathscr{R}$ is the spectral resolving power and $\Omega$ is the solid angle subtended by a monochromatic ring at an angle $\theta$ defined by the full-width half-maxima (FWHM) intensities. This is a statement of the Jacquinot relation $\mathscr{R}\Omega = 2\pi$ which has been used to demonstrate that the throughput of the Fabry-Perot exceeds the throughput of slit-aperture devices by almost two orders of magnitude (Jacquinot 1954). This advantage is realized when observing diffuse sources which extend over large solid angles. For an instrumental finesse $\mathscr{N}$, we find that $\Omega = 2\pi\,\theta\,\delta\theta = \pi\lambda(\mathscr{N}\mu l)^{-1}$ such that the solid angles subtended by successive rings across a monochromatic source are constant, and therefore have equal spectroscopic resolution. For an unresolved emission line, the signal-to-noise ratio (SNR) in a Fabry-Perot ring after combining $f$ CCD exposures is given by

$$\mathrm{SNR} = s(\epsilon\tau\eta)^{0.5}\left(\frac{\delta\lambda}{\Gamma}\right)^{0.5}\left(\frac{\Omega}{\omega}\right)^{0.5}[s + b + f\Gamma(\epsilon\tau\,\delta\lambda)^{-1}\sigma_R^2]^{-0.5}, \tag{2}$$

where $s$ and $b$ are the source and background flux (counts pixel$^{-1}$ s$^{-1}$); $\epsilon$ and $\tau$ are the efficiency and exposure times, respectively; and $\omega$ is the solid angle subtended by a pixel. It is important to note that, for a given instrumental profile FWHM, $\Gamma$, the Airy profile allows 50% more light through the spectrograph when compared to spectrometers with Gaussian instrumental profiles (Bland-Hawthorn 1994). The factor $\eta$ corrects for a calculation based on the FWHM of a ring and is defined as the ratio of the photometric bandpass and the instrumental FWHM. We normally choose to place the ring center at one corner of the field for two reasons. First, it is *always* necessary to tilt the etalon in order to throw ghost light out of the field. Secondly, the factor $(\Omega/\omega)^{0.5}$ in equation (2) now ensures that the spectroscopic sensitivity is constant over most of the field. In our experiment, each monochromatic ring subtends roughly 2600 arcsec$^2$. However, there is an almost linear dropoff in sensitivity at large off-axis angles (northwest field) where the rings become seriously incomplete.

The observations described in § 2 were taken through a $50 \times 50$ mm filter and a 50 mm diameter etalon stopped down to 45 mm. These optics restrict, respectively, the field and aperture area available to TAURUS-2 which has a 60 mm diameter pupil and an unvignetted field of 80 mm diameter at the focal plane. The projected 16 mm diameter Cassegrain hole at the pupil is particularly severe (30% loss) in the stopped beam. Our 75 mm diameter etalons and filters increase the effective aperture and projected solid angle for an Airy ring by factors of 2.1 and 2.4, respectively. For a dark sky and using the 75 mm optics, we find that TAURUS-2 can reach an Hα emission measure[1] of $E_m = 0.02\,\mathrm{cm}^{-6}$ pc at the 3 $\sigma$ level in about 6 hr across the full free spectral range (57 Å). This photometric limit is much more sensitive than related experiments to date (Kutryev & Reynolds 1989; Songaila, Bryant, & Cowie 1989; Williams & Schommer 1993) and can be achieved without compromise from the instrumental artefacts which have traditionally plagued Fabry-Perot observations. It would be difficult to improve on this performance at other telescopes although marginal improvements are possible at lower orders of interference. There are several possible sources of systematic error including CCD fringes, extraneous etalon fringes, and in the transformation from Cartesian to polar coordinates. But these can be ameliorated with adequate calibrations, e.g., flat fields with pixel-to-pixel uncertainties of less than 0.1%. Due to an oversight, the flat field obtained for the 3C 273 observations was significantly worse than this which forced us to smooth the image (see § 3), thereby producing weak systematic variations in the residual spectrum (Fig. 2).

## 6. IMPLICATIONS

In an important paper, Hogan & Weymann (1987) have suggested that deep observations of blank sky might reveal patches of optical line emission, specifically redshifted Lyα emission, from quasar absorption-line clouds irradiated by the metagalactic UV background. We have repeated their calculation for both Hα and Lyα with recent measurements of the background at the Lyman limit ($\nu = \nu_0$). If we assume that the metagalactic flux has a $\nu^{-1}$ spectrum at energies greater than $h\nu_0$, we find

$$E_m \approx \frac{CJ_{-21}}{(1+\mathscr{Z})^3}\left(\frac{N_{\mathrm{H\,I}}}{10^{17}\,\mathrm{cm}^{-2}}\right)\mathrm{cm}^{-6}\,\mathrm{pc}, \tag{3}$$

where $\mathscr{Z}$ is redshift and $C$ is 0.6 and 0.05 for Lyα and Hα, respectively. $J_{-21}$ is the specific intensity of the ionizing flux at

[1] We have adopted an electron temperature of $10^4$ K.

the Lyman limit in units of $10^{-21}$ ergs cm$^{-2}$ s$^{-1}$ sr$^{-1}$ Hz$^{-1}$, and $N_{\rm H\,I}$ is the (optically thin) column density of neutral hydrogen. If the clouds are made of primordial material, the $H^+$ electron temperatures could be as high as 40,000 K which would effectively double $E_m$.

The proximity effect in the Ly$\alpha$ forest has been used to estimate $J_{-21}$ at different mean redshifts: 0.006 ($\mathscr{Z} \sim 0.5$; Kulkarni & Fall 1993), 1 ($\mathscr{Z} \sim 2.8$; Bajtlik, Duncan, & Ostriker 1988), and 0.2 ($\mathscr{Z} \sim 4.2$; Williger et al. 1994). An upper limit of $J_{-21} < 0.6$ has been obtained from direct measurement by the Ultraviolet Spectrometer on board *Voyager 2* (Holberg 1986, 1990) although more stringent limits have been set by other authors (Henry 1991; Bowyer 1991).

It is unlikely that Ly$\alpha$ emission will be detectable since, to be observable in the optical, it would need to be substantially redshifted ($\mathscr{Z} > 2.5$) at which point the clouds are very faint and unlikely to fill the available field (9′). The relative frequency of absorption lines scales as $N_{\rm H\,I}^{-1.7}$ (Carswell et al. 1984) and, when the proximity effect is correctly accounted for, the redshift distribution scales as roughly $(1 + \mathscr{Z})^{2.3}$ (Bajtlik 1993). Ly$\alpha$ absorption line systems lie in the range $10^{13} < N_{\rm H\,I} < 10^{17}$ cm$^{-2}$ and so are unlikely to be detectable in H$\alpha$ at any redshift. A small fraction of intergalactic absorbers (1%) have larger column densities, and these typically correspond to metal systems at significant redshift (Lanzetta 1993). Equation (3) differs from the optically thick limit by a factor of 0.25 for the case of plane parallel radiative transfer. Roughly speaking, if we take the transitional column density to be $5 \times 10^{17}$ cm$^{-2}$ and an intermediate local value of $J_{-21} = 0.06$, then $E_m(\mathrm{H}\alpha) \sim 0.05$ cm$^{-6}$ pc for $N_{\rm H\,I} > 10^{18}$ cm$^{-2}$. Thus, it is within the realm of possibility that high column density clouds will ultimately be detected in H$\alpha$ at low redshift, assuming that they are sufficiently extended.

Our new deep limit of $E_m(\mathrm{H}\alpha) \approx 0.02$ cm$^{-6}$ pc has important consequences for other experiments. High-velocity clouds have been used to probe the metagalactic ionizing radiation field although, to date, only marginal detections have been possible (Kutryev & Reynolds 1989; Songaila et al. 1989). The number of ionizing photons streaming into one hemisphere of the Galactic halo from the disk is roughly $2.2 \times 10^6 e^{-|z|/1\ \mathrm{kpc}}$ photons cm$^{-2}$ s$^{-1}$ (Sokolowski 1994), where $|z|$ is the height out of the plane, such that for an optically thin cloud,

$$E_m(\mathrm{H}\alpha) \approx 2.0\left(\frac{N_{\rm H\,I}}{10^{17}\ \mathrm{cm}^{-2}}\right) e^{-|z|/1\ \mathrm{kpc}}\ \mathrm{cm}^{-6}\ \mathrm{pc}\ . \qquad (4)$$

Wakker (1991) has recently cataloged clouds with large column densities which have been observed at radio wavelengths with adequate resolution (~2′). Some of these are presumably at high enough latitudes ($|z| > 3$ kpc) to probe the cosmic ionizing flux unambiguously. Our improved performance means that a statistically useful number (~$10^2$) of these clouds can now be reached. This has already been partly realized with TAURUS-2 at the AAT where our superior spectral baseline has now permitted the simultaneous detection of more than one emission line from at least one high-velocity cloud in Wakker's list.

Arguably, the most important experiment which becomes possible at our new deep limit is the detection of ionized gas beyond the H I truncation radius in spiral galaxies (Corbelli & Salpeter 1993; Maloney 1993). Sunyaev (1969) first argued that the H I disks of spiral galaxies truncate at a few times the optical diameter because the exponentially declining H I column eventually becomes fully ionized by the metagalactic radiation field. Our most recent observations with TAURUS-2 (in collaboration with K. C. Freeman and P. J. Quinn) were motivated by the models of Maloney (1993) which give the expected H$\alpha$ emission measure at the truncation point in NGC 3198 ($N_{\rm H\,I} \approx 5 \times 10^{19}$ cm$^{-2}$) for different values of $J_{-21}$ (0.04, 0.08, 0.2). The most conservative model predicts values of $E_m(\mathrm{H}\alpha)$ in the range 0.02–0.06 cm$^{-6}$ pc. In principle, these outer $H^+$ disks could allow us to probe the dark halo potential out to scales (>30 kpc) beyond the reach of H I rotation curves.

We are most grateful to John Webb for his thoughtful comments on an early draft of this *Letter*. An anonymous referee also made a number of very useful suggestions. We would like to acknowledge R. S. Ellis and G. J. Ferland for their assistance. We are particularly grateful to R. D. Cannon for the opportunity to fully calibrate the TAURUS-2 system and to R. B. Tully for the loan of the HIFI etalon and filters.

## REFERENCES

Bahcall, J. N., et al. 1991, ApJ, 377, L5
Bajtlik, S. 1993, in The Environment and Evolution of Galaxies, ed. J. M. Shull & H. A. Thronson (Dordrecht: Kluwer), 191
Bajtlik, S., Duncan, R. C., & Ostriker, J. P. 1988, ApJ, 327, 580
Bland, J., & Tully, R. B. 1989, AJ, 98, 723
Bland-Hawthorn, J. 1994, in IAU Colloq. 149, Tridimensional Optical Spectroscopic Methods in Astrophysics, ed. G. Comte & M. Marcelin, in press
Bowyer, S. 1991, ARA&A, 29, 59
Carswell, R. F., et al. 1984, ApJ, 278, 486
Corbelli, E., & Salpeter, E. E. 1993, ApJ, 419, 104
Henry, R. C. 1991, ARA&A, 29, 89
Hogan, C. J., & Weymann, R. J. 1987, MNRAS, 225, 1P
Holberg, J. B. 1986, ApJ, 311, 969
———. 1990, in IAU Symp. 139, The Galactic and Extragalactic Background, ed. S. Bowyer & C. Leinert (Dordrecht: Kluwer), 220
Jacquinot, P. 1954, J. Opt. Soc. Am., 44, 761
Kulkarni, V. P., & Fall, S. M. 1993, ApJ, 413, L63
Kutryev, A. S., & Reynolds, R. J. 1989, ApJ, 344, L9
Lanzetta, K. M. 1993, in The Environment and Evolution of Galaxies, ed. J. M. Shull & H. A. Thronson (Dordrecht: Kluwer), 237
Maloney, P. 1993, ApJ, 414, 41
Morris, S. L., et al. 1991, ApJ, 377, L21
Osterbrock, D. E., & Martel, A. 1992, PASP, 101, 76
Sokolowski, J. 1994, ApJ, submitted
Songaila, A., Bryant, W., & Cowie, L. L. 1989, ApJ, 345, L71
Sunyaev, R. 1969, Astrophys. Lett., 3, 69
Taylor, K., & Atherton, P. D. 1980, MNRAS, 191, 675
Wakker, B. P. 1991, A&A, 250, 484
Weymann, R. J. 1993, in The Environment and Evolution of Galaxies, ed. J. M. Shull & H. A. Thronson (Dordrecht: Kluwer), 213
Williams, T. B., & Schommer, R. 1993, ApJ, 419, L53
Williger, G., et al. 1994, ApJ, 428, 574